

Optimize Wider, Not Deeper: Consensus Aggregation for Policy Optimization

Zelal Su (Lain) Mustafaoglu¹, Sungyoung Lee², Eshan Balachandar¹,
Risto Miikkulainen¹, Keshav Pingali¹

Keywords: RL, On-Policy RL, Policy Optimization, Trust Region Methods, Proximal Policy Optimization (PPO), Natural Gradients, Information Geometry, Continuous Control

Summary

Proximal policy optimization (PPO) approximates the trust region update using multiple epochs of clipped SGD. Each epoch may drift further from the natural gradient direction, creating path-dependent noise. To understand this drift, we can use Fisher information geometry to decompose policy updates into *signal* (the natural gradient projection) and *waste* (the Fisher-orthogonal residual that consumes trust region budget without first-order surrogate improvement). Empirically, signal saturates but waste grows with additional epochs, creating an *optimization-depth dilemma*. We propose **Consensus Aggregation for Policy Optimization (CAPO)**, which redirects compute from depth to width: K PPO replicates are optimized on the same batch, differing only in minibatch shuffling order, and then aggregated into a consensus. We study aggregation in two spaces: Euclidean parameter space, and the natural parameter space of the policy distribution via the logarithmic opinion pool. In natural parameter space, the consensus provably achieves higher KL-penalized surrogate and tighter trust region compliance than the mean expert; parameter averaging inherits these guarantees approximately. On continuous control tasks, CAPO outperforms PPO and compute-matched deeper baselines under fixed sample budgets by up to $8.6\times$. CAPO demonstrates that policy optimization can be improved by optimizing wider, rather than deeper, without additional environment interactions.

Contribution(s)

1. A Fisher-geometric decomposition of the PPO update into signal (natural gradient projection) and waste (Fisher-orthogonal residual). Signal saturates within a few epochs while waste accumulates, formalizing the optimization-depth dilemma.
Context: The decomposition explains why increasing epoch count yields diminishing returns and why averaging PPO copies improves KL efficiency: shared signal is preserved while path-dependent waste partially cancels.
2. CAPO (Consensus Aggregation for Policy Optimization) algorithm: runs the PPO inner loop K times independently on the same batch and aggregates them into a consensus, either in parameter space or in the natural parameter space of the policy distribution.
Context: In natural parameter space, the consensus provably achieves higher KL-penalized surrogate and tighter trust region compliance than the mean expert (Theorem 2). The natural-parameter consensus is exactly the LogOP, which outperforms Euclidean averaging when expert variances diverge.
3. Empirical validation across continuous control benchmarks in Gymnasium, providing empirical insights into signal-waste decomposition and demonstrating improvements over PPO and compute-matched baselines.
Context: CAPO outperforms PPO on five out of six tasks by up to $8.6\times$, while PPO with $K\times$ more epochs degrades on every task due to waste accumulation. Parameter averaging reduces waste by 2–17%, across all tasks; aggregation in natural parameter space (LogOP) achieves 46% waste reduction on Humanoid, where precision-weighting across more parameters amplifies the benefit due to the high dimensionality of the task.

Optimize Wider, Not Deeper: Consensus Aggregation for Policy Optimization

Zelal Su (Lain) Mustafaoglu¹, Sungyoung Lee², Eshan Balachandar¹, Risto Miikkulainen¹, Keshav Pingali¹

zsm@utexas.edu, sylee@utexas.edu, eshan@cs.utexas.edu,
risto@cs.utexas.edu, pingali@cs.utexas.edu

¹Department of Computer Science, University of Texas at Austin ²Department of Electrical and Computer Engineering, University of Texas at Austin

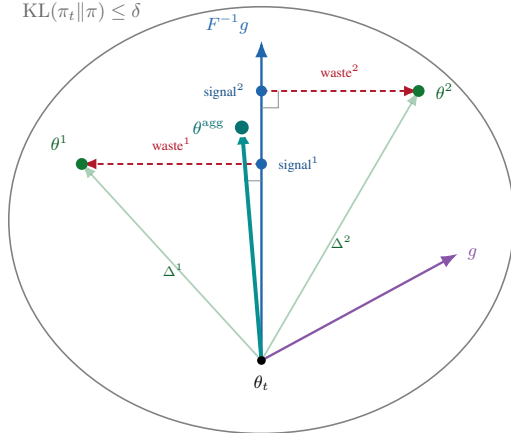
Abstract

Proximal policy optimization (PPO) approximates the trust region update using multiple epochs of clipped SGD. Each epoch may drift further from the natural gradient direction, creating path-dependent noise. To understand this drift, we can use Fisher information geometry to decompose policy updates into *signal* (the natural gradient projection) and *waste* (the Fisher-orthogonal residual that consumes trust region budget without first-order surrogate improvement). Empirically, signal saturates but waste grows with additional epochs, creating an *optimization-depth dilemma*. We propose **Consensus Aggregation for Policy Optimization (CAPO)**, which redirects compute from depth to width: K PPO replicates are optimized on the same batch, differing only in minibatch shuffling order, and then aggregated into a consensus. We study aggregation in two spaces: Euclidean parameter space, and the natural parameter space of the policy distribution via the logarithmic opinion pool. In natural parameter space, the consensus provably achieves higher KL-penalized surrogate and tighter trust region compliance than the mean expert; parameter averaging inherits these guarantees approximately. On continuous control tasks, CAPO outperforms PPO and compute-matched deeper baselines under fixed sample budgets by up to 8.6 \times . CAPO demonstrates that policy optimization can be improved by optimizing wider, rather than deeper, without additional environment interactions.

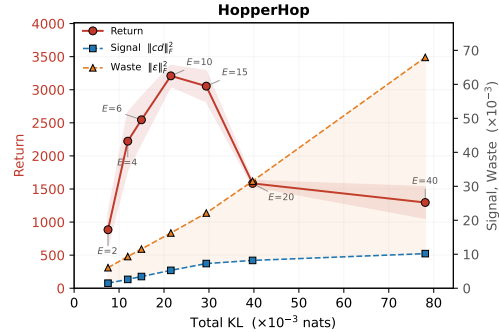
1 Introduction

Policy gradient methods are used in reinforcement learning to train policies for tasks in problem domains ranging from robotics (Rudin et al., 2022) to large language model alignment (Ouyang et al., 2022). A neural network called the *policy network* is used to map each state s to a distribution $\pi(\cdot|s)$ over actions, and the distribution is sampled to determine the next action for the agent. The objective of training is to find values for policy network parameters θ^* that maximize the expected total reward.

Like most complex nonlinear optimization problems, this problem has to be solved using heuristic search. The initial point θ_0 in the parameter space is usually chosen heuristically, and some rule is used iteratively to move from the current search point θ_t to the next search point θ_{t+1} (by convention, a subscript always refer to a timestep but we omit the subscript when it is obvious from the context). It is useful to think of this move as choosing a *direction* followed by a *step* in that direction. The move can be guided by the value of the function (and gradient, if available) at the previous and current time-steps. The notation π_t refers to the policy induced by the policy network parameters θ_t at step t .



(a) Signal–waste decomposition in the trust region.



(b) Return, signal, waste vs. total KL of the final PPO update. (Hopper, 3 seeds). Return (red, left axis) peaks at $E = 10$ then collapses; signal KL (blue) saturates while waste KL (orange) grows $11\times$.

Figure 1: **Geometry of CAPO updates.** (a) REINFORCE moves along the gradient g (solid) (approximately), while TRPO moves along the natural gradient $F^{-1}g$ (approximately). Each PPO expert’s move Δ^k decomposes into a *signal* (•, projection onto $F^{-1}g$) and *waste* (dashed, Fisher-orthogonal residual). In this diagram, waste points left for expert θ^1 and right for expert θ^2 so averaging reduces waste, and the consensus θ^{agg} lies closer to $F^{-1}g$ with lower KL than either expert (Theorem 2). (b) Return and signal–waste KL decomposition of the final PPO update for varying epoch counts E on Hopper, mean over 3 seeds. Return peaks at $E = 10$ then collapses as waste overwhelms the trust region budget.

The classic REINFORCE method (Sutton & Barto, 1998) uses a Monte Carlo estimate of the gradient at θ_t , and moves in the direction of the gradient with a step size determined by a heuristic learning rate. In Figure 1a, this direction is shown conceptually by the line labeled g . Although easy to implement, the gradient estimates have high variance so moves made by REINFORCE are noisy.

This problem led to the development of *trust region methods* like TRPO (Schulman et al., 2015), which introduces explicit proximity constraints on updates to determine step sizes in a more principled way. TRPO requires the expectation of the KL-divergence $D_{KL}(\pi_t(s), \pi_{t+1}(s))$ over all states s (written as $\overline{KL}(\pi_t, \pi_{t+1})$), to be bounded, making policy optimization a *constrained* optimization problem. Following Amari & Nagaoka (2000), Kakade (2001) showed that the optimal direction for this problem is the *natural gradient* $F^{-1}g$ where F is the Fisher information matrix and g is the gradient. Intuitively, the natural gradient is the direction of steepest improvement per unit of KL-divergence cost, and is shown by the line labeled $F^{-1}g$ in Figure 1(a). TRPO computes this direction approximately using the conjugate gradient method followed by a backtracking line search, which is computationally expensive. In contrast, PPO (Schulman et al., 2017) trades trust region optimality for efficiency and reduced complexity by approximating the update with E epochs of clipped minibatch SGD, with M minibatches per epoch. This simplification comes at a cost: each additional epoch may drift further from the natural gradient direction. As a result, PPO is a *noisy estimator* of the KL-constrained natural gradient step.

Using Fisher information geometry, we can decompose any update into a *signal* component, which is the projection onto the natural gradient, and an orthogonal *waste* component, as shown in Figure 1a for two updates θ^1 and θ^2 (projection is made more precise in Section 2.2 using Fisher inner product). Correspondingly, the KL cost of the update splits into signal KL and waste KL (Proposition 1). Figure 1b shows the KL cost decomposition for the *final* PPO update¹ for Hopper, a standard control benchmark. Each point is PPO using a different epoch count E ; the x -axis is the total KL cost. Return (red, left axis) peaks at $E = 10$ and collapses beyond it. The right axis decomposes total KL cost into signal KL, (blue, $\|cd\|_F^2$) and waste KL (orange, $\|\epsilon\|_F^2$). Signal KL saturates after

¹To be precise, this is the update from θ_{f-1} to θ_f where θ_f is the final search point.

a few epochs, but waste KL grows $11\times$ from $E = 2$ to $E = 40$, consuming the trust region budget without contributing to the surrogate gain.

The classical remedy for reducing noise is to average estimates. **CAPO** (Consensus Aggregation for Policy Optimization) does exactly this: given a fixed batch, it runs K copies of the PPO optimizer, with the same data and incumbent but different minibatch orderings, and aggregates them into a single consensus policy. The aggregation can be performed in parameter space or in the natural parameter space of the policy distribution via the logarithmic opinion pool. In both cases, waste partially cancels while signal is preserved, as shown by the point labeled θ^{agg} in Figure 1a.

Our contributions are:

1. **Signal-waste decomposition** (Section 2.2): A Fisher-geometric decomposition of the noisy PPO update that formalizes the optimization-depth dilemma and explains why compute-matched optimization (PPO- $K\times$) degrades.
2. **CAPO: a consensus operator for trust region policy optimization** (Section 3). K PPO copies on the same batch, aggregated into a consensus that provably improves on the mean individual expert in both surrogate value and trust region compliance (Theorem 2).
3. **Empirical validation** (Section 5):
 - CAPO (LogOP) outperforms PPO and compute-matched baselines on five out of six Gymnasium continuous control benchmarks by up to $+71\%$ on low-dimensional tasks and $8.6\times$ on Humanoid, a high-dimensional task.
 - Parameter averaging reduces waste by 2–17%, across all tasks; aggregation in natural parameter space (LogOP) achieves 46% waste reduction on Humanoid, where precision-weighting across more parameters amplifies the benefit due to the high dimensionality of the task.
 - The only overhead is $K\times$ gradient computation, which is embarrassingly parallel and requires no additional environment interaction. As a result, end-to-end time increases only by about 25% on the average even for $K = 4$ (Section B.2).

2 Preliminaries

This section describes TRPO and PPO formally, and motivates CAPO.

2.1 Trust Region Policy Optimization

The KL-constrained trust region policy optimization step can be described concisely as follows: if the current policy is π_t , find π_{t+1} that maximizes the expectation shown below, subject to the bound on the expected KL-divergence between π_t and π_{t+1} .

$$\pi_{t+1} = U_{\delta}^*(\pi_t, \mathcal{B}) = \arg \max_{\pi} \hat{\mathbb{E}}_{s, a \sim \mathcal{B}} \left[\frac{\pi(a|s)}{\pi_t(a|s)} \hat{A}^{\pi_t}(s, a) \right] \quad \text{s.t.} \quad \overline{\text{KL}}(\pi_t || \pi) \leq \delta. \quad (1)$$

Here, \mathcal{B} is the batch collected by the current policy π_t , the trust region bound is δ , and \hat{A} are advantages for (state, action) pairs estimated via generalized advantage estimation (GAE) (Schulman et al., 2016). Computing U_{δ}^* exactly is intractable, so this optimization problem is solved approximately.

TRPO (Schulman et al., 2015) solves a quadratic approximation (the surrogate) to (1) using the Fisher information matrix $F(\theta) = \mathbb{E}_{s, a \sim \pi_{\theta}} [\nabla \log \pi_{\theta}(a|s) \nabla \log \pi_{\theta}(a|s)^{\top}]$, which captures the local curvature of the policy’s distribution space. The KL constraint becomes $\frac{1}{2} \Delta^{\top} F \Delta \leq \delta$, where Δ is the update, yielding the natural gradient direction $\Delta^* \propto F^{-1}g$. TRPO computes the update direction via conjugate gradient, and then performs a line search.

PPO (Schulman et al., 2017) replaces the KL constraint with a clipped surrogate:

$$L^{\text{CLIP}}(\theta) = \hat{\mathbb{E}}_t \left[\min \left(\rho_t(\theta) \hat{A}_t, \text{clip}(\rho_t(\theta), 1-\epsilon, 1+\epsilon) \hat{A}_t \right) \right], \quad (2)$$

where $\rho_t(\theta) = \pi(a_t|s_t)/\pi_t(a_t|s_t)$ is the importance sampling ratio and ϵ is the clip threshold. PPO runs E epochs of minibatch SGD (M minibatches per epoch, yielding EM sequential gradient steps). This is computationally cheaper than TRPO but only approximately enforces the trust region: clipping truncates large likelihood ratios but does not bound KL divergence. The gap between TRPO’s geometrically principled update and PPO’s approximation is what CAPO exploits.

2.2 The Optimization-Depth Dilemma

To determine much of PPO’s update is wasted, it is useful to compute the Fisher signal–waste decomposition, defined formally below.

Definition 1 (Fisher signal–waste decomposition). *Let $\hat{d} = F^{-1}g / \|F^{-1}g\|_F$ be the unit natural gradient direction in the Fisher norm $\|v\|_F = \sqrt{v^\top F v}$. Any update $\Delta = (\theta - \theta_t)$ decomposes uniquely as*

$$\Delta = \underbrace{c \hat{d}}_{\text{signal}} + \underbrace{\epsilon}_{\text{waste}}, \quad c = \langle \Delta, \hat{d} \rangle_F, \quad \langle \epsilon, \hat{d} \rangle_F = 0, \quad (3)$$

where $\langle u, v \rangle_F = u^\top F v$ is the Fisher inner product and c is the projection on the natural gradient.

The consensus update decomposes as $\bar{\Delta} = \bar{c} \hat{d} + \bar{\epsilon}$ with $\bar{c} = \frac{1}{K} \sum_k c^k$ and $\bar{\epsilon} = \frac{1}{K} \sum_k \epsilon^k$.

To keep the notation simple, we use c and ϵ for projections and residuals of both the updates and the total KL since the context and type always makes it clear which one is being referred to. Signal KL and waste KL are measured in KL units ($\times 10^{-3}$ nats). We define *Fisher alignment* $\alpha = c^2 / (c^2 + \|\epsilon\|_F^2)$ to measure the fraction of the total KL budget spent on the natural gradient direction. *Fisher cosine similarity* $\text{cos}_F(\Delta) = \langle \Delta, \hat{d} \rangle_F / \|\Delta\|_F$ measures directional alignment.

Proposition 1 (Signal–waste separation). *Under decomposition (3):*

- (i) **First-order surrogate improvement depends only on signal.** $g^\top \Delta = c \|F^{-1}g\|_F$. The waste ϵ contributes nothing.
- (ii) **KL cost is additive.** $\frac{1}{2} \Delta^\top F \Delta = \frac{1}{2} c^2 + \frac{1}{2} \|\epsilon\|_F^2$. The signal costs $\frac{1}{2} c^2$ in KL; the waste costs $\frac{1}{2} \|\epsilon\|_F^2$ in KL with no first-order return.

Proof. Using $g = \|F^{-1}g\|_F * F \hat{d}$ and $\Delta_k = c_k \hat{d} + \epsilon_k$:

$$(i) \quad g^\top \Delta_k = c_k \|F^{-1}g\|_F \underbrace{\hat{d}^\top F \hat{d}}_1 + \|F^{-1}g\|_F \underbrace{\hat{d}^\top F \epsilon_k}_0 = c_k \|F^{-1}g\|_F.$$

(ii) By Pythagoras’s theorem in the Fisher norm (Amari & Nagaoka (2000)): $\Delta_k^\top F \Delta_k = c_k^2 + \|\epsilon_k\|_F^2$ (cross-term vanishes by orthogonality). \square

In theory, TRPO has $\epsilon = 0$ by construction since it follows the natural gradient $F^{-1}g$. PPO experts have $\epsilon \neq 0$.

Table 1 tracks signal KL and waste KL as E varies on the Gymnasium Hopper task with (64, 64) networks². At $E = 4$, alignment is $\alpha = 0.22$: only 22% of the KL budget produces surrogate improvement; the remaining 78% is waste. Increasing depth (E) does not help; waste grows 11× from $E = 2$ to $E = 40$, alignment never exceeds 0.25, and the returns peak at $E \approx 10$ before collapsing. The dilemma is clear: PPO cannot spend its KL budget efficiently no matter how many epochs it runs.

²Figure 1b showed this data pictorially.

Table 1: **Signal KL and waste KL vs. epoch count.** Fisher decomposition of the final PPO update at varying epoch counts. Hopper, Gymnasium, (64, 64) network, 3 seeds. Signal c^2 and waste $\|\epsilon\|_F^2$ in 10^{-3} KL-nats.

Epochs E	Return	Signal c^2	Waste $\ \epsilon\ _F^2$	Total KL	α	cos_F
2	884 \pm 304	1.5	6.0	7.5	0.20	0.43
4	2222 \pm 529	2.6	9.3	11.9	0.22	0.46
6	2546 \pm 430	3.4	11.5	15.0	0.23	0.47
10	3210 \pm 193	5.3	16.3	21.5	0.24	0.49
15	3054 \pm 286	7.2	22.1	29.4	0.25	0.49
20	1584 \pm 55	8.2	31.5	39.7	0.21	0.45
40	1296 \pm 292	10.1	67.9	78.0	0.13	0.35

2.3 Motivation for CAPO

This limitation of PPO motivates replacing depth with width: rather than running one optimizer like PPO for KE epochs, run K experts for E epochs each and average the results; waste partially cancels while signal is preserved. The remaining question is how to create the K experts. Since collecting samples through environment interactions is the performance bottleneck, we cannot afford to collect an on-policy batch for each expert.

CAPO exploits the following insight. Abstractly, the output of an approximate optimizer like PPO is a *random variable*; different minibatch orderings, initializations, and accumulation paths yield different final policies. This randomness is not negligible. [Henderson et al. \(2018\)](#) show that implementation details and random seeds dominate RL outcomes, and policy gradient estimates are known to be high-variance ([Ilyas et al., 2020](#)).

CAPO focuses on one specific source of randomness: the minibatch ordering across PPO’s E epochs of SGD. Unlike TRPO, PPO’s output depends on the minibatch ordering: given the same batch \mathcal{B} and incumbent π_t , different shuffles produce different policies. As SGD processes minibatches sequentially, these orthogonal gradient components accumulate into the waste vector. Each minibatch ordering accumulates a different sequence of gradient steps, producing substantially different waste vectors (Section 5.3, Supplementary A), yielding different experts.

Section 3 develops this idea.

3 CAPO: Consensus Aggregation for Policy Optimization

Although we focus on PPO in this paper, the idea behind CAPO is quite general and can be used with other trust region methods. Given an optimizer U and a current policy π_t , CAPO collects a batch of data \mathcal{B} under π_t , and then generates K CAPO experts π^1, \dots, π^K with copies of the current incumbent policy parameters θ_t and Adam optimizer state ([Kingma & Ba, 2015](#)), but using different minibatch orderings.

This approach ensures that any variation across experts is due to the optimization path, not the data. The K expert policies are then aggregated into a consensus π^{agg} , which serves as the next policy π_{t+1} . The incumbent’s optimizer state is carried forward unchanged (while there are other design choices, this default worked well in our experiments, as shown in Supplementary C.1). This process is repeated for multiple generations until convergence or the sample budget is exhausted. Figure 2 shows this dataflow.

The remaining design choice is the choice of space in which to average. The simplest option is Euclidean parameter space (CAPO-Avg):

$$\theta_{t+1} = \theta_t + \frac{1}{K} \sum_{k=1}^K (\theta^k - \theta_t). \tag{4}$$

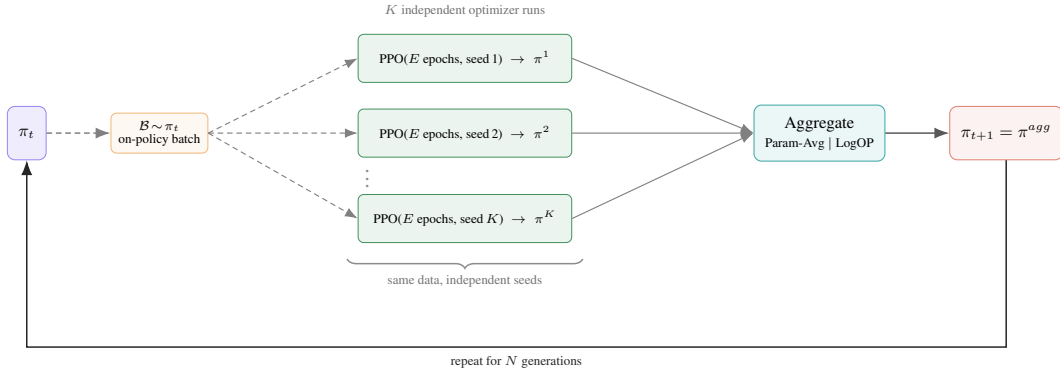


Figure 2: **CAPO pipeline.** One on-policy batch is collected from the incumbent π_t and fed to K independent PPO copies that differ only in minibatch shuffle order. Expert policies are aggregated into a consensus π_{t+1} in parameter space (avg) or distribution space (LogOP).

Alternatively, one can aggregate in distribution space via the logarithmic opinion pool (LogOP) (Genest & Zidek, 1986; Heskes, 1997), which averages expert policies in the natural parameter space:

$$q(a|s) \propto \prod_{k=1}^K \pi^k(a|s)^{1/K}. \quad (5)$$

For any exponential family, this product stays in the same family: if each expert has natural parameters η^k , then q has natural parameters $\bar{\eta} = \frac{1}{K} \sum_k \eta^k$ (the average across the K experts), so q is a proper, closed-form distribution. For diagonal Gaussian experts $\pi^k(\cdot|s) = \mathcal{N}(\mu^k, \text{diag}(\sigma^{k2}))$, this gives a Gaussian consensus with *precision-weighted* parameters:

$$\mu_q = \left(\sum_k \frac{1}{\sigma^{k2}} \right)^{-1} \sum_k \frac{\mu^k}{\sigma^{k2}}, \quad \sigma_q^{-2} = \frac{1}{K} \sum_k \sigma^{k-2}, \quad (6)$$

where all operations are element-wise over action dimensions. An expert with lower variance (higher precision σ^{-2}) on an action dimension pulls the consensus mean more strongly on that dimension: the LogOP automatically upweights confident experts per dimension, unlike parameter averaging which weights all experts equally. Since q is a per-state analytic distribution, not a neural network, it is distilled into π_{t+1} by minimizing $\text{KL}(q||\pi_{t+1})$ with a line search that rejects any step where $\text{KL}(\pi_t||\pi_{t+1}) > \delta$. We refer to this variant as **CAPO** and treat it as the default algorithm.

The two consensus rules obviously coincide when expert variances are identical. Although experts usually stay close to π_t within the trust region, there is a small but non-zero gap. Empirically, LogOP outperforms parameter averaging on five of six tasks (Section 5.2).

Pseudocode for CAPO is provided in Algorithm 1. The computational overhead is $K \times$ gradient computation per generation, no additional environment interaction, and $1 \times$ inference cost (Table 2).

Budget allocation. A fraction f_w of the total step budget C is spent on PPO warmup to initialize the incumbent. The remaining $(1-f_w)C$ steps are divided across G generations, each collecting one on-policy batch of B frames and running K expert updates in parallel on that batch. Because experts share the same batch, the per-expert sample budget is $(1-f_w)C/G$, identical to single-expert PPO, while gradient compute scales as $K \times$. The warmup fraction trades initial policy quality against the number of aggregation generations; we ablate this tradeoff in Section C.2.3, and default to 10% in our experiments.

Expert diversity. In our current configuration, the sole source of expert diversity is minibatch ordering: each expert receives a different shuffle seed, producing different minibatch sequences

Algorithm 1 CAPO: Consensus Aggregation for Policy Optimization

Require: Budget T , experts K , PPO epochs E

- 1: Initialize policy π_0 , value function V_0 , optimizer state ϕ_0
 - 2: Optional warmup: standard PPO until return exceeds floor
 - 3: **for** generation $g = 0, 1, 2, \dots$ until budget exhausted **do**
 - 4: Collect batch $\mathcal{B} \sim \pi_t$ (C frames); compute \hat{A} via GAE(λ)
 - 5: **for** $k = 1, \dots, K$ **in parallel do**
 - 6: $\theta^k \leftarrow \theta_t, \phi^k \leftarrow \phi_t$ {Copy incumbent}
 - 7: Run E PPO epochs with shuffle seed $k \rightarrow \theta^k$
 - 8: **end for**
 - 9: $\theta_{t+1} \leftarrow \text{Aggregate}(\theta^1, \dots, \theta^K)$ {Avg or LogOP}
 - 10: $\phi_{t+1} \leftarrow \phi_t$ {Carry incumbent optimizer state}
 - 11: Update value function V on \mathcal{B} {Trained once, not replicated}
 - 12: **end for**
-

 Table 2: **Compute comparison.** CAPO trades parallel gradient computation for reduced update variance, without additional environment frames or inference cost.

Method	Env. Frames	Grad. Steps	Inference	Update Quality
PPO	C	EM	$1\times$	Baseline
PPO- $K\times$ (more epochs)	C	$K \cdot EM$	$1\times$	Degrades
PPO-SWA	C	EM	$1\times$	Moderate
Best-of- K	C	$K \cdot EM$	$1\times$	Selection only
Ensemble Methods	C	$K \cdot EM$	$K\times$	Moderate
CAPO (Ours)	C	$K \cdot EM$	$1\times$	Best

through the same data. Optionally, experts can also use different GAE λ values, giving each expert a different advantage estimate and thus a different optimization target. We leave this for future work.

4 Consensus Improvement Theorem

Theorem 2 formalizes the benefit of consensus aggregation. We state it in natural parameter space η where the KL bound is exact (exponential families generalize Gaussians).

Theorem 2 (Consensus improvement in natural parameter space). *Let π_t belong to a minimal exponential family with natural parameters η_t and log-partition function $A(\eta)$. Let η^1, \dots, η^K be expert natural parameters and $\bar{\eta} = \frac{1}{K} \sum_k \eta^k$. Then:*

- (a) **Averaging preserves expected improvement.** *The linearized surrogate $\hat{L}_{\text{lin}}(\eta) = g_\eta^\top(\eta - \eta_t)$, where $g_\eta = \nabla_\eta L^{\text{surr}}|_{\eta_t}$, is linear in η . Therefore $\hat{L}_{\text{lin}}(\bar{\eta}) = \frac{1}{K} \sum_k \hat{L}_{\text{lin}}(\eta^k)$.*
- (b) **Averaging reduces KL cost (exactly).** $\text{KL}(\pi_t \| \pi_{\bar{\eta}}) = D_A(\eta, \eta_t)$ is convex in η since $\nabla^2 A(\eta) = F(\eta) \succeq 0$. Jensen’s inequality gives:

$$\text{KL}(\pi_t \| \pi_{\bar{\eta}}) \leq \frac{1}{K} \sum_k \text{KL}(\pi_t \| \pi_{\eta^k}).$$

Unlike the quadratic Fisher approximation $\frac{1}{2} \Delta^\top F \Delta$, this is exact.

- (c) **Better improvement per unit of KL.** For any $\lambda > 0$, the KL-penalized surrogate $J_\lambda(\eta) = \hat{L}_{\text{lin}}(\eta) - \lambda \text{KL}(\pi_t \| \pi_\eta)$ satisfies

$$J_\lambda(\bar{\eta}) \geq \frac{1}{K} \sum_k J_\lambda(\eta^k).$$

- (d) **Trust region compliance.** The sublevel set $\mathcal{C}_\delta = \{\eta : \text{KL}(\pi_t \| \pi_\eta) \leq \delta\}$ is convex. If each $\eta^k \in \mathcal{C}_\delta$, then $\bar{\eta} \in \mathcal{C}_\delta$.

Proof. (a) $\hat{L}_{\text{lin}}(\eta) = g_{\eta}^{\top}(\eta - \eta_t)$ is linear in η , so $\hat{L}_{\text{lin}}(\bar{\eta}) = \frac{1}{K} \sum_k \hat{L}_{\text{lin}}(\eta_k)$.

(b) $\text{KL}(\pi_t \| \pi_{\eta}) = D_A(\eta, \eta_t)$ is a Bregman divergence of the convex log-partition $A(\eta)$. Jensen’s inequality gives $D_A(\bar{\eta}, \eta_t) \leq \frac{1}{K} \sum_k D_A(\eta_k, \eta_t)$.

(c) $J_{\lambda}(\bar{\eta}) = \hat{L}_{\text{lin}}(\bar{\eta}) - \lambda \text{KL}(\pi_t \| \pi_{\bar{\eta}}) = \frac{1}{K} \sum_k \hat{L}_{\text{lin}}(\eta_k) - \lambda \text{KL}(\pi_t \| \pi_{\bar{\eta}}) \geq \frac{1}{K} \sum_k J_{\lambda}(\eta_k)$, using (a) and (b).

(d) $\mathcal{C}_{\delta} = \{\eta : D_A(\eta, \eta_t) \leq \delta\}$ is convex (sublevel set of a convex function), so $\eta_k \in \mathcal{C}_{\delta} \forall k \implies \bar{\eta} \in \mathcal{C}_{\delta}$. \square

Remark 1 (Connection to the Fisher decomposition). *In parameter space, the quadratic approximation $\text{KL} \approx \frac{1}{2} \Delta^{\top} F \Delta$ yields $J_{\lambda}(\bar{\Delta}) - \frac{1}{K} \sum_k J_{\lambda}(\Delta^k) = \frac{\lambda}{2} [\text{Var}(c^k) + \frac{1}{K} \sum_k \|\epsilon^k - \bar{\epsilon}\|_F^2]$. Signal variance is empirically small, so waste reduction drives the gain. Alignment $\alpha(\bar{\Delta}) > \frac{1}{K} \sum_k \alpha(\Delta^k)$ follows when $\text{Var}(c^k) \ll \bar{c}^2$.*

The following corollary summarizes the key takeaway.

Corollary 3 (Consensus is a better policy improvement step). *Let experts η^1, \dots, η^K each lie within the trust region ($\text{KL}(\pi_t \| \pi_{\eta^k}) \leq \delta$). The natural-parameter consensus $\bar{\eta} = \frac{1}{K} \sum_k \eta^k$ simultaneously:*

- (i) *achieves higher KL-penalized surrogate than the mean expert: $J_{\lambda}(\bar{\eta}) \geq \frac{1}{K} \sum_k J_{\lambda}(\eta^k)$;*
- (ii) *stays within the trust region: $\text{KL}(\pi_t \| \pi_{\bar{\eta}}) \leq \frac{1}{K} \sum_k \text{KL}(\pi_t \| \pi_{\eta^k}) \leq \delta$.*

For CAPO-Avg, these guarantees hold approximately in parameter space. For CAPO, they hold exactly for the analytic log opinion pool barycenter q ; the distilled neural policy π_{t+1} inherits them up to distillation error.

5 Experiments

The results in this section show that the theoretical benefits of consensus aggregation translate to improved returns on continuous control benchmarks.

5.1 Setup and Environments

We implement CAPO in Gymnasium MuJoCo-v4 using (64, 64) networks following CleanRL (Huang et al., 2022), with $K = 4$ experts by default (ablated in Supplementary C.2). We evaluate on six continuous control tasks (Table 3), reporting mean episodic return over 20 evaluation episodes.

Table 3: **Evaluation environments.** Task type, state and action space dimensions. All tasks use Gymnasium MuJoCo-v4.

Environment	Type	dim(\mathcal{S})	dim(\mathcal{A})
Hopper	Hopping locomotion	11	3
HalfCheetah	Locomotion	17	6
Walker2d	Locomotion	17	6
Ant	Multi-legged locomotion	27	8
Humanoid	High-dim locomotion	376	17
HumanoidStandup	High-dim balance	376	17

We compare the two CAPO aggregation operators, **CAPO** and **CAPO-Avg** against five baselines including **PPO** (Schulman et al., 2017) and **TRPO** (Schulman et al., 2015). The other three baselines are **PPO- $K\times$** , which runs PPO with KE epochs on the same batch, matching CAPO’s total gradient cost but spending it sequentially, **Best-of- K** , which trains K independent PPO copies and selects the one with the highest surrogate, isolating selection from averaging, and **PPO-SWA** (stochastic weight averaging (Izmailov et al., 2018) along the PPO trajectory).

5.2 Main Results

Table 4: **Returns on Gymnasium** (mean \pm SE, 8 seeds, (64, 64) MLP, 1M steps; Humanoid at 4M). \dagger Compute-matched ($K\times$ gradient budget). Bold = best per task.

Method	Hopper	HalfCheetah	Walker2d	Ant	Humanoid	HumanoidStandup
PPO	2711 \pm 268	1604 \pm 28	2518 \pm 280	2142 \pm 97	739 \pm 39	143k \pm 3k
PPO- $K\times$ \dagger	1210 \pm 304	1532 \pm 91	1432 \pm 337	232 \pm 21	429 \pm 11	104k \pm 5k
Best-of- K \dagger	2255 \pm 274	1940 \pm 294	3770 \pm 341	1664 \pm 241	716 \pm 41	145k \pm 4k
PPO-SWA	2240 \pm 307	1261 \pm 431	1010 \pm 127	943 \pm 88	750 \pm 55	121k \pm 6k
TRPO	2583 \pm 300	1629 \pm 27	3441 \pm 303	1029 \pm 102	3730 \pm 339	134k \pm 4k
CAPO-Avg \dagger	3193\pm93	1967 \pm 260	3223 \pm 354	1738 \pm 185	696 \pm 28	141k \pm 5k
CAPO\dagger	2397 \pm 286	2737\pm373	3871\pm275	2328\pm194	6367\pm196	149k\pm3k

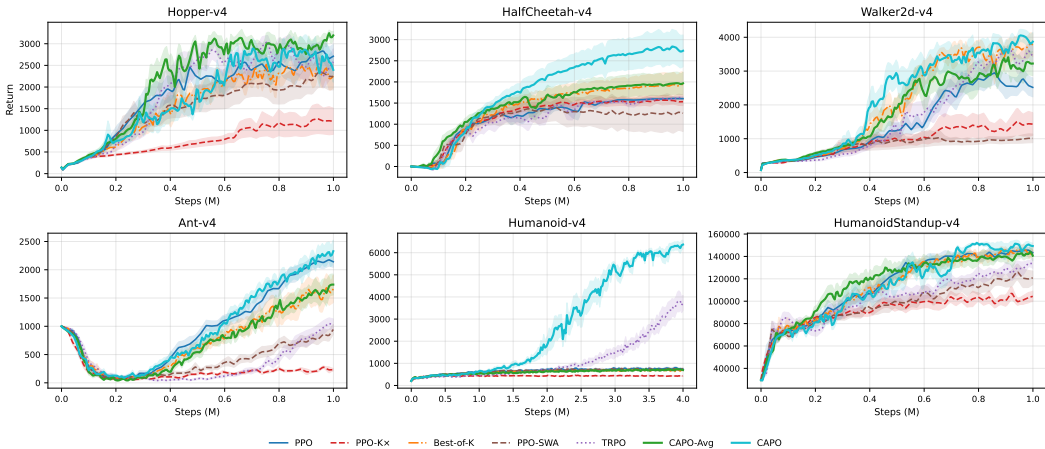


Figure 3: **Gymnasium learning curves** (8 seeds, shaded ± 1 SE). CAPO leads on all tasks except Hopper, which is dominated by CAPO-Avg. PPO- $K\times$ collapses on Ant (7 \times below PPO) and Walker2d, validating the optimization-depth dilemma.

Figure 3 shows learning curves for all methods; Table 4 shows final evaluation results. CAPO beats baselines on all tasks except Hopper, which CAPO-Avg dominates. The largest gains are on HalfCheetah (2737, +71% over PPO) and Walker2d (3871, +54%).

On Ant, CAPO (2328) exceeds PPO (2142). On Hopper, CAPO-Avg (3193) achieves the highest return while CAPO (2397) is comparable to PPO (2463); this low-dimensional task limits the benefit of precision-weighting. On Humanoid, CAPO (6367) achieves 8.6 \times the return of PPO (739); TRPO (3730) also benefits strongly, while CAPO-Avg (696) remains near PPO parity, demonstrating that LogOP’s per-dimension precision-weighting is beneficial in high-dimensional action spaces over longer horizons. On HumanoidStandup, CAPO outperforms all baselines.

PPO- $K\times$ degrades on every task, most catastrophically on Ant (232, 9 \times below PPO), confirming the depth dilemma. PPO-SWA also degrades, confirming that trajectory averaging is insufficient. Best-of- K improves over PPO on some tasks but inherits the selected expert’s full waste. Wall clock overhead is modest: \sim 0–40% for CAPO-Avg, 19–72% for CAPO (Supplementary B.2).

5.3 Fisher Decomposition Diagnostics

We validate the empirical behavior predicted by the Fisher decomposition.

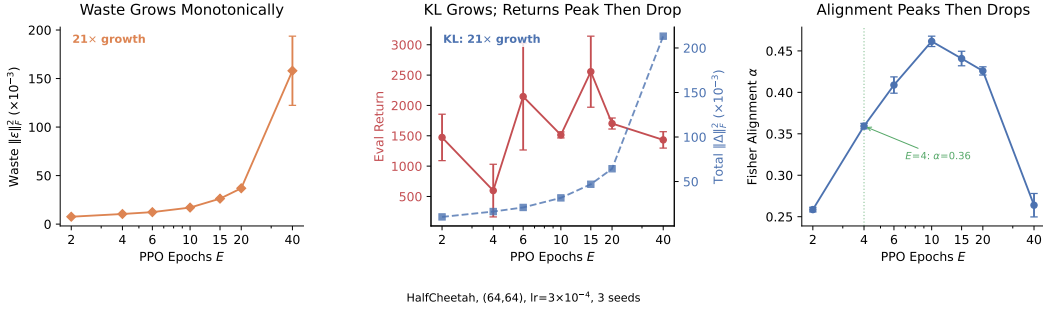


Figure 4: **Fisher diagnostics for the last PPO update vs. epoch count** (HalfCheetah, (64, 64) network, 3 seeds). Left: waste $\|\epsilon\|_F^2$ and signal c^2 on log scale. Center: total KL and return. Right: Fisher alignment. Waste grows 21 \times from $E = 2$ to $E = 40$; returns peak at $E \approx 6-15$ then decline; alignment α peaks at 0.46 then drops to 0.26.

(i) **KL waste dominates as number of epochs grow:** Section 2.2 showed this on Hopper (Table 1); Figure 4 confirms the pattern on HalfCheetah. At $E = 4$, waste accounts for 64% of the total KL update ($\alpha = 0.36$). Waste grows 21 \times from $E = 2$ to $E = 40$ without plateauing; signal also grows but slower. Fisher alignment α peaks at $E \approx 10$ ($\alpha = 0.46$) then drops to 0.26 at $E = 40$; the returns peak early ($E \approx 6-15$) and decline as total KL overshoots the trust region.

(ii) **Waste is less correlated than signal** (Table 5): signal correlation $\rho_c > 0.99$ while waste correlation $\rho_\epsilon \in [0.77, 0.97]$.

(iii) **Averaging directly reduces waste** (Table 6): CAPO-Avg reduces waste by 2–17%, with the largest reduction on Humanoid. On low-dimensional tasks, LogOP amplifies waste (5–9 \times) but improves returns nevertheless. On high-dimensional tasks (Ant, Humanoid) it reduces waste, confirming that LogOP’s gains come from precision weighting.

Full tables and methodology for (ii) and (iii) in Supplementary A.

5.4 Ablations

We ablate four design choices in Supplementary C: **optimizer state carry** (Section C.1), **clip threshold** ϵ (Section C.2.1), **KL early stopping** (Section C.2.2), and **warm-up budget** (Section C.2.3); and **width scaling** (Section C.2), varying K at fixed epoch count E . The key findings are:

1. **Width scales; depth does not.** Increasing K at fixed E improves returns monotonically (CAPO) or up to $K = 8$ (CAPO-Avg), whereas increasing E past ~ 10 degrades all methods.
2. **CAPO is robust to trust region parameters.** CAPO maintains strong performance across a range of clipping and KL early stopping thresholds. PPO’s own performance is sensitive to these choices (e.g., dropping 3 \times on Walker2d when ϵ deviates from 0.2), while CAPO tolerates a wider operating range.
3. **Warmup and optimizer carry are secondary.** Performance varies modestly across warmup fractions (0–20%) and carry modes; the default 10% warmup with incumbent carry is a reasonable choice across tasks.

6 Related Work

CAPO draws on several research threads, primarily weight averaging in optimization, and ensemble and population-based methods in RL.

Weight averaging in optimization. SWA (Izmailov et al., 2018), Lookahead (Zhang et al., 2019), and Nikishin et al. (2018) average along a single optimization trajectory; CAPO averages across K parallel trajectories, which cancels path-dependent waste that temporal averaging preserves (PPO-SWA degrades in performance, as shown in Table 4). SWAP (Gupta et al., 2020) averages parallel workers on the same data with different minibatch orderings, the closest supervised-learning analog to CAPO, but lacks trust region structure or Fisher-geometric analysis. Model soups (Wortsman et al., 2022), WARP (Rame et al., 2024), and Rewarded Soups (Rame et al., 2023) average across hyperparameters or reward models; CAPO averages across optimization paths from the *same* hyperparameters and objective, isolating optimizer noise as the diversity source. One-shot averaging (Zinkevich et al., 2010), local SGD (Stich, 2019), and DiLoCo (Douillard et al., 2023) average parallel workers with heterogeneous data; CAPO operates on homogeneous data where all diversity comes from the optimizer, making the signal–waste decomposition tractable.

Ensemble and population methods in RL. EPPO (Yang et al., 2022) maintains K policies at inference time ($K\times$ inference cost); CAPO aggregates at optimization time and deploys a single policy ($1\times$ inference). CEM-RL (Pourchot & Sigaud, 2019), ERL (Khadka & Tumer, 2018), and EPO (Mustafaoglu et al., 2025) combine evolutionary perturbations with gradients; CAPO requires no random perturbations, deriving all diversity from stochastic optimization paths. Qiu et al. (2025) scale ES to multi-billion-parameter LLM fine-tuning via many simple perturbation steps; CAPO takes fewer, gradient-informed steps and exploits curvature via the natural gradient. SVPG (Liu et al., 2017) maintains diverse particles via repulsive kernels; CAPO aggregates into a single consensus without explicit repulsion.

7 Discussion and Future Work

CAPO exploits the structure of optimizer noise in trust region optimization: signal saturates early while waste accumulates with additional epochs, so averaging parallel copies cancels waste while preserving signal. The principle generalizes: in any setting where iterative refinement on fixed data produces diminishing-return noise, width-first strategies may offer better variance-bias tradeoffs.

Practical tips for practitioners. For PPO, returns peak at an epoch count of 10, and degrade significantly by $E=20$. Implementing KL early stopping (ablated in 5.4) is recommended. $K=8$ yields the best returns, but $K=4$ was used in our experiments to handle the efficiency/performance trade-off.

Limitations. $K\times$ gradient cost is the primary overhead, though expert training is embarrassingly parallel and wall-clock time scales sublinearly with K . All experiments use continuous control with Gaussian policies; the theory applies to exponential families generally, but we have no empirical evidence for discrete actions, vision, or language tasks.

Future work. Future work could explore principled methods for generating diverse experts for increased waste reduction. We also explored richer diversity sources beyond minibatch ordering, such as Bayesian bootstrap reweighting of advantages and diverse GAE lambda values, which increase expert disagreement but introduce estimator heterogeneity not covered by Theorem 2. The signal–waste decomposition suggests CAPO could improve LLM fine-tuning, where optimizer noise compounds across long sequences.

Broader Impact Statement

CAPO reduces costly environment interactions, potentially accelerating robotics and simulation-based RL research.

References

- Shun-ichi Amari and Hiroshi Nagaoka. *Methods of Information Geometry*, volume 191 of *Translations of Mathematical Monographs*. American Mathematical Society and Oxford University Press, Providence, RI, 2000. ISBN 0-8218-0531-2. Translated from the 1993 Japanese original by Daishi Harada.
- Arthur Douillard, Qixuan Feng, Andrei A Rusu, Serkan Cabi, Sherjil Ozair, Nicolas Heess, and Razvan Pascanu. DiLoCo: Distributed low-communication training of language models. In *NeurIPS Workshop on Efficient Natural Language and Speech Processing*, 2023.
- Christian Genest and James V. Zidek. Combining probability distributions: A critique and an annotated bibliography. *Statistical Science*, 1(1):114–148, 1986. DOI: 10.1214/ss/1177013825.
- Vipul Gupta, Tomer Koren, and Yoram Singer. Stochastic weight averaging in parallel: Large-batch training that generalizes well. In *International Conference on Learning Representations*, 2020.
- Peter Henderson, Riashat Islam, Philip Bachman, Joelle Pineau, Doina Precup, and David Meger. Deep reinforcement learning that matters. In *Proceedings of the AAAI Conference on Artificial Intelligence (AAAI)*, 2018.
- Tom Heskes. Selecting weighting factors in logarithmic opinion pools. In *Advances in Neural Information Processing Systems 10 (NeurIPS 1997)*, 1997.
- Shengyi Huang et al. Cleanrl: High-quality single-file implementations of deep reinforcement learning algorithms. *Journal of Machine Learning Research*, 2022.
- Andrew Ilyas et al. A closer look at deep policy gradients. In *International Conference on Learning Representations (ICLR)*, 2020.
- Pavel Izmailov, Dmitrii Podoprikin, Timur Garipov, Dmitry Vetrov, and Andrew Gordon Wilson. Averaging weights leads to wider optima and better generalization. In *Conference on Uncertainty in Artificial Intelligence*, 2018.
- Sham M. Kakade. A natural policy gradient. In *Advances in Neural Information Processing Systems 14 (NeurIPS 2001)*, 2001.
- Shauharda Khadka and Kagan Tumer. Evolutionary reinforcement learning. *arXiv preprint arXiv:1805.07917*, 2018.
- Diederik P. Kingma and Jimmy Ba. Adam: A method for stochastic optimization. In *International Conference on Learning Representations (ICLR)*, 2015.
- Qiang Liu, Changyou Chen, Chang Wang, and Jun Zhu. Stein variational policy gradient. *arXiv preprint arXiv:1704.02399*, 2017.
- Zelal Su Mustafaoglu et al. Evolutionary policy optimization, 2025. Preprint / to appear.
- Evgenii Nikishin et al. Improving stability in deep reinforcement learning with weight averaging. *arXiv preprint*, 2018.
- Long Ouyang, Jeffrey Wu, Xu Jiang, Diogo Almeida, Carroll Wainwright, Pamela Mishkin, Chong Zhang, Sandhini Agarwal, Katarina Slama, Alex Ray, et al. Training language models to follow instructions with human feedback. *Advances in Neural Information Processing Systems*, 35: 27730–27744, 2022.
- Antoine Pourchot and Olivier Sigaud. CEM-RL: Combining evolutionary and gradient-based methods for policy search. *arXiv preprint arXiv:1810.01222*, 2019.

-
- Xin Qiu, Yulu Gan, Conor F. Hayes, Qiyao Liang, Elliot Meyerson, Babak Hodjat, and Risto Miikkulainen. Evolution strategies at scale: LLM fine-tuning beyond reinforcement learning. *arXiv preprint arXiv:2509.24372*, 2025.
- Alexandre Rame, Guillaume Couairon, Laure Soulier, and Matthieu Cord. Rewarded soups: Towards Pareto-optimal alignment by interpolating weights fine-tuned on diverse rewards. In *Advances in Neural Information Processing Systems*, 2023.
- Alexandre Rame, Guillaume Couairon, Corentin Dancette, Jean-Baptiste Gaya, Laure Soulier, and Matthieu Cord. WARP: On the benefits of weight averaged rewarded policies. *arXiv preprint arXiv:2406.16768*, 2024.
- Nikita Rudin, David Hoeller, Philipp Reist, and Marco Hutter. Learning to walk in minutes using massively parallel deep reinforcement learning. In *Conference on Robot Learning*, pp. 91–100. PMLR, 2022.
- John Schulman, Sergey Levine, Pieter Abbeel, and Michael I. Jordan. Trust region policy optimization. In *Proceedings of the 32nd International Conference on Machine Learning (ICML)*, 2015.
- John Schulman, Philipp Moritz, Sergey Levine, Michael I. Jordan, and Pieter Abbeel. High-dimensional continuous control using generalized advantage estimation. *arXiv preprint arXiv:1506.02438*, 2016.
- John Schulman, Filip Wolski, Prafulla Dhariwal, Alec Radford, and Oleg Klimov. Proximal policy optimization algorithms. *arXiv preprint arXiv:1707.06347*, 2017.
- Sebastian U. Stich. Local SGD converges fast and communicates little. *ICLR*, 2019.
- Richard S. Sutton and Andrew G. Barto. *Reinforcement Learning: An Introduction*. The MIT Press, Cambridge, MA, 1998.
- Mitchell Wortsman, Gabriel Ilharco, Samir Yitzhak Gadre, Rebecca Roelofs, Raphael Gontijo-Lopes, Ari S. Morcos, Hongseok Namkoong, Ali Farhadi, Yair Carber, Simon Kornblith, and Ludwig Schmidt. Model soups: Averaging weights of multiple fine-tuned models improves accuracy without increasing inference time. In *Proceedings of the 39th International Conference on Machine Learning*, volume 162, pp. 23965–23998. PMLR, 2022.
- Zhengyu Yang, Kan Ren, Xufang Luo, Minghuan Liu, Weiqing Liu, Jiang Bian, Weinan Zhang, and Dongsheng Li. Towards applicable reinforcement learning: Improving the generalization and sample efficiency with policy ensemble. In *Proceedings of the Thirty-First International Joint Conference on Artificial Intelligence (IJCAI-22)*, pp. 3659–3665, jul 2022. DOI: 10.24963/ijcai.2022/508.
- Michael R. Zhang, James Lucas, Geoffrey Hinton, and Jimmy Ba. Lookahead optimizer: k steps forward, 1 step back. In *Advances in Neural Information Processing Systems*, volume 32, 2019.
- Martin Zinkevich, Markus Weimer, Lihong Li, and Alex Smola. Parallelized stochastic gradient descent. In *Advances in Neural Information Processing Systems (NeurIPS)*, 2010.

Supplementary Materials

The following content was not necessarily subject to peer review.

A Fisher Decomposition Diagnostics

This appendix extends the empirical analysis of Sections 2.2 and 5.3, and presents full Fisher decomposition diagnostics: signal–waste correlation, and direct waste reduction measurement.

A.1 Signal/Waste Correlation

Table 5 breaks down the signal and waste correlation at the final generation for CAPO-Avg.

Table 5: **Signal vs. waste correlation at the final generation** ($K = 4$), CAPO-Avg. Gymnasium, (64, 64) network, 5 seeds.

Environment	ρ_c (signal)	ρ_ϵ (waste)	ρ_{total}	\bar{c}/\bar{c}_k
HalfCheetah	0.999	0.974	0.976	0.999
Walker2d	0.999	0.961	0.966	0.999
Hopper	0.993	0.934	0.939	0.995
Ant	1.000	0.969	0.973	1.000
Humanoid	1.000	0.774	0.837	1.000

Waste correlation ρ_ϵ ranges from 0.77 (Humanoid) to 0.97 (HalfCheetah).

A.2 Waste Reduction

The correlation analysis above predicts waste cancellation; we now measure it directly. We decompose the consensus update Δ_{cons} into signal and waste using the same Fisher projection, and report the ratio $\|\epsilon_{\text{cons}}\|_F^2 / \frac{1}{K} \sum_k \|\epsilon_k\|_F^2$ in Table 6. A ratio below 1 means the consensus has less waste than the average expert; above 1 means waste was amplified.

Table 6: **Direct waste reduction: consensus vs. PPO** ($K = 4$, $E = 10$). Ratio $\|\bar{\epsilon}\|_F^2 / \frac{1}{K} \sum_k \|\epsilon_k\|_F^2$ measures how much waste the consensus retains relative to PPO. Values < 1 : waste reduced; values > 1 : waste amplified. d_s : observation dimension; d_a : action dimension. Gymnasium, (64, 64) network, 5 seeds.

Environment	Method	d_s	d_a	$\frac{1}{K} \sum_k \ \epsilon_k\ _F^2$	$\ \bar{\epsilon}\ _F^2$	Ratio
Hopper	CAPO-Avg	11	3	7.8×10^{-4}	7.4×10^{-4}	0.950 ± 0.015
Hopper	CAPO	11	3	1.3×10^{-3}	6.5×10^{-3}	5.68 ± 1.31
HalfCheetah	CAPO-Avg	17	6	2.7×10^{-3}	2.7×10^{-3}	0.980 ± 0.003
HalfCheetah	CAPO	17	6	3.5×10^{-3}	2.4×10^{-2}	9.27 ± 2.46
Walker2d	CAPO-Avg	17	6	1.1×10^{-3}	1.1×10^{-3}	0.971 ± 0.005
Walker2d	CAPO	17	6	9.7×10^{-4}	7.6×10^{-3}	8.37 ± 1.13
Ant	CAPO-Avg	27	8	8.8×10^{-2}	8.0×10^{-2}	0.914 ± 0.001
Ant	CAPO	27	8	6.9×10^{-2}	3.7×10^{-2}	0.668 ± 0.004
Humanoid	CAPO-Avg	376	17	0.342	0.285	0.832 ± 0.002
Humanoid	CAPO	376	17	0.058	0.032	0.559 ± 0.022

CAPO-Avg reduces waste on every environment, with reduction scaling with parameter count: 2% on HalfCheetah/Walker2d ($n_\theta = 17$), 5% on Hopper ($n_\theta = 11$), and 17% on Humanoid ($n_\theta =$

376). This directly confirms the theoretical prediction that averaging cancels waste while preserving signal.

CAPO (LogOP) demonstrates a striking pattern: it amplifies waste 5–10 \times on low-dimensional tasks ($n_\theta \leq 17$), but achieves 33% waste reduction on Ant ($d_s = 27$) and 46% waste reduction on Humanoid ($n_\theta = 376$). This illustrates how the benefits from precision-weighting scale with the dimensionality of the task.

B Experimental Details

This section presents all hyperparameters used in the experiments, and reports a comparison of wall-clock time for all methods.

B.1 Hyperparameters

B.1.1 CAPO Hyperparameters

Parameter	Default	Description
K (n_experts)	4 (see Section C.2)	Number of parallel expert policies per generation
Carry policy	incumbent	Optimizer state carryover between generations

B.1.2 PPO Hyperparameters

Parameter	Value	Description
Hidden layers	(64, 64)	Policy and value network
Activation	tanh	Hidden layer activation
Initialization	Orthogonal	Weight init method
Std parameterization	clip	Log-std to std conversion
Learning rate	3×10^{-4}	Adam LR (policy and value)
Adam ϵ	10^{-5}	Adam epsilon
LR annealing	linear $\rightarrow 0$	Over total optimization steps
Discount γ	0.99	Return discount factor
GAE λ	0.95	Generalized advantage estimation
Clip ϵ	0.2	PPO clipping threshold
Entropy coef.	0.0	Entropy bonus coefficient
VF coef.	0.5	Value loss coefficient
Max grad norm	0.5	Global gradient norm clipping
PPO epochs E	10	Gradient passes per rollout
Minibatches	32	Per epoch
Rollout horizon H	512	Steps per environment
Parallel envs	8	Training environments

B.1.3 Base Optimizer Hyperparameters

Parameter	Default	Description
base_optimizer	ppo	$\in \{\text{ppo}, \text{trpo}\}$
trpo_damping	0.1	Fisher-vector product damping for CG (TRPO only)
trpo_cg_iters	10	Max conjugate gradient iterations (TRPO only)

B.2 Wall-Clock Timing

APO’s $K\times$ gradient cost is the primary overhead. Table 7 reports wall-clock times on Gymnasium. CAPO-Avg adds $\sim 0\text{--}40\%$ wall-clock overhead despite $4\times$ gradient cost, because CAPO’s fewer generations amortize overhead (JIT recompilation, env resets, evaluation). CAPO adds 19–72% due

to the distillation step. Notably, PPO- $K\times$ is often *slower* (21–65% overhead) because its sequential epochs cannot be parallelized.

Table 7: Wall-clock time on Gymnasium, 8 seeds. PPO row: absolute seconds (mean \pm SE). Other rows: ratio to PPO (\times). Five tasks at 1M steps; Humanoid at 4M[†].

	HalfCheetah	Walker2d	Ant	Hopper	Humanoid [†]	HumanoidStandup
PPO	1331 \pm 155	1376 \pm 179	1563 \pm 247	1027 \pm 8	6756 \pm 837	1629 \pm 82
PPO- $K\times$	1.37 \times	1.36 \times	1.38 \times	1.41 \times	1.21 \times	1.65 \times
TRPO	0.98 \times	0.99 \times	1.03 \times	1.01 \times	1.02 \times	0.95 \times
PPO-SWA	0.97 \times	0.99 \times	1.04 \times	1.00 \times	0.92 \times	1.06 \times
Best-of- K	1.36 \times	1.31 \times	1.18 \times	1.67 \times	1.06 \times	1.01 \times
CAPO-Avg	1.12 \times	1.16 \times	0.96 \times	1.40 \times	0.99 \times	1.00 \times
CAPO	1.54 \times	1.72 \times	1.39 \times	1.42 \times	1.19 \times	1.28 \times

C Ablations and Scaling

C.1 Optimizer State Carry

Table 8: Optimizer state carry ablation: CAPO-Avg and CAPO across three Gymnasium environments (1M steps, 3 seeds, mean \pm SE). Bold indicates the best carry mode per row.

Method	Env	Incumbent	Reset	Best Expert	Average
CAPO-Avg	Hopper	2836 \pm 521	2991 \pm 260	2513 \pm 268	2868 \pm 415
	Walker2d	3823 \pm 338	2689 \pm 934	4066 \pm 140	3836 \pm 238
	Ant	1647 \pm 337	1517 \pm 234	2580 \pm 266	2534 \pm 240
CAPO	Hopper	2041 \pm 530	2697 \pm 578	2640 \pm 831	1757 \pm 182
	Walker2d	3312 \pm 1052	3153 \pm 738	2924 \pm 1072	3197 \pm 592
	Ant	2496 \pm 407	2016 \pm 257	2328 \pm 90	2229 \pm 34

No carry mode dominates consistently (Table 8). Each generation, K experts train independently from a shared Adam state, building up their own momentum over E epochs. In *incumbent* mode, expert optimizer states are discarded after aggregation; the pre-generation state is kept with only the step counter advanced so the learning rate schedule decays correctly. Since the momentum and second-moment buffers are never updated between generations, incumbent carry is effectively equivalent to *reset* (both start each generation with zero momentum). The two modes differ only in that reset re-initializes the optimizer object, and indeed they perform comparably across all six settings. *Best-expert* carry inherits one expert’s Adam momentum, creating a potential mismatch when the next generation trains from the *consensus* parameters; surprisingly, it performs well for CAPO-Avg (best on Walker2d and Ant), suggesting that the winning expert’s curvature estimate transfers usefully under parameter averaging. *Average* carry, which averages second moments across divergent gradient histories, is competitive for CAPO-Avg but consistently weak for CAPO (LogOP). Overall, the choice of carry mode is secondary to the aggregation method itself; we retain incumbent as the default for simplicity.

C.2 Width Scaling: Varying K

The epoch sweep (Section 2.2) shows that deeper optimization hits diminishing returns. The complementary question is: does wider optimization (more experts K at fixed epoch count E) continue to improve? We run CAPO-Avg with $K \in \{2, 4, 8, 16\}$ at $E = 10$ on Gymnasium, so that total gradient cost scales linearly with K .

Both methods are stable across K . On Walker2d, CAPO-Avg peaks at $K = 8$ (4279) and remains above the PPO baseline at all widths; CAPO peaks at $K = 8$ as well (4056). On HalfCheetah, CAPO-Avg peaks at $K = 8$ (3116) but drops at $K = 16$ (1746), while CAPO improves monotonically up

Table 9: Width scaling: CAPO and CAPO-Avg with varying K at fixed $E = 10$. Gymnasium, 1M steps, 3 seeds, mean \pm SE.

	$K=2$	$K=4$	$K=8$	$K=16$
<i>HalfCheetah</i>				
CAPO	2491 \pm 824	2382 \pm 765	3022 \pm 668	3556 \pm 965
CAPO-Avg	2021 \pm 319	2510 \pm 728	3116 \pm 562	1746 \pm 52
<i>Walker2d</i>				
CAPO	3549 \pm 530	2587 \pm 176	4056 \pm 93	3585 \pm 558
CAPO-Avg	3361 \pm 164	3609 \pm 239	4279 \pm 344	3523 \pm 34
<i>Ant</i>				
CAPO	2346 \pm 310	1939 \pm 96	2356 \pm 189	2801 \pm 227
CAPO-Avg	1675 \pm 341	1392 \pm 71	1840 \pm 252	1564 \pm 64

to $K = 16$ (3556). On Ant, CAPO scales well with width (2801 at $K = 16$), while CAPO-Avg peaks at $K = 8$ (1840). In all cases, width scaling does not degrade performance, in contrast to the catastrophic effect of increasing E past 10.

C.2.1 Clip Threshold ϵ

Table 10 varies the PPO clip threshold.

Table 10: Clip threshold ablation ($\epsilon \in \{0.1, 0.2, 0.3, 0.5\}$). Gymnasium, 1M steps, 3 seeds, mean \pm SE.

	$\epsilon=0.1$	$\epsilon=0.2$	$\epsilon=0.3$	$\epsilon=0.5$
<i>HalfCheetah</i>				
PPO	1726 \pm 126	1568 \pm 196	1165 \pm 38	1068 \pm 91
CAPO-Avg	1560 \pm 17	3176 \pm 959	1631 \pm 45	1809 \pm 213
CAPO	1760 \pm 151	2374 \pm 480	2035 \pm 415	2067 \pm 767
<i>Walker2d</i>				
PPO	1544 \pm 479	932 \pm 223	894 \pm 90	462 \pm 34
CAPO-Avg	2539 \pm 727	2626 \pm 159	3011 \pm 819	2890 \pm 423
CAPO	865 \pm 79	3850 \pm 611	4001 \pm 404	2759 \pm 838
<i>Ant</i>				
PPO	503 \pm 78	316 \pm 47	201 \pm 72	68 \pm 16
CAPO-Avg	990 \pm 40	1588 \pm 187	1930 \pm 426	1163 \pm 396
CAPO	849 \pm 163	2212 \pm 9	2323 \pm 45	2593 \pm 398

PPO degrades monotonically as ϵ increases on all three environments: from 1726 to 1068 on HalfCheetah, 1544 to 462 on Walker2d, and 503 to 68 on Ant. Larger ϵ permits larger policy ratio deviations per epoch, compounding overshoot across multiple epochs. CAPO-Avg and CAPO (LogOP) are substantially more robust: CAPO-Avg stays above 1560 on HalfCheetah and above 2539 on Walker2d across the full range. On Ant, CAPO (LogOP) actually improves with ϵ (849 \rightarrow 2593), suggesting that the consensus mechanism can exploit larger per-expert updates when precision-weighting neutralizes the noise they introduce.

C.2.2 KL Early Stopping

Table 11 tests KL early stopping, which caps the number of epochs per iteration when a KL threshold is exceeded.

PPO on Ant is extremely sensitive to the KL threshold: it achieves 2142 only at $\text{tkl}=0.02$ and collapses to 295–823 at all other settings, a $\sim 7\times$ performance range. CAPO-Avg and CAPO (LogOP) are far more robust, staying above 1550 and 1851 respectively across all settings. On HalfCheetah and Walker2d, PPO likewise performs best at $\text{tkl}=0.02$ (the only setting that prevents catastrophic

Table 11: KL early stopping ablation ($\text{target_kl} \in \{0, 0.02, 0.04, 0.08\}$). Gymnasium, 1M steps, 3 seeds, mean \pm SE.

	tkl=0	tkl=0.02	tkl=0.04	tkl=0.08
<i>HalfCheetah</i>				
PPO	1475 \pm 114	2922 \pm 756	2166 \pm 346	1355 \pm 56
CAPO-Avg	2522 \pm 992	1579 \pm 30	2532 \pm 814	1943 \pm 399
CAPO	2274 \pm 676	2361 \pm 821	1967 \pm 282	2307 \pm 664
<i>Walker2d</i>				
PPO	664 \pm 94	3281 \pm 339	1204 \pm 188	1454 \pm 254
CAPO-Avg	3160 \pm 1100	4408 \pm 242	3955 \pm 189	2490 \pm 776
CAPO	3444 \pm 714	3371 \pm 675	3345 \pm 505	3680 \pm 578
<i>Ant</i>				
PPO	295 \pm 78	2142 \pm 28	823 \pm 89	406 \pm 34
CAPO-Avg	1552 \pm 258	2367 \pm 123	2224 \pm 346	1701 \pm 187
CAPO	1851 \pm 203	2676 \pm 344	2643 \pm 104	2304 \pm 197

overshoot without being overly conservative), while both CAPO variants maintain competitive performance across the full range. Combined with the clip threshold results, this confirms that consensus aggregation stabilizes PPO against hyperparameter sensitivity.

C.2.3 Warmup Budget

Table 12 varies the fraction of the total step budget allocated to warmup PPO before expert averaging begins.

Table 12: Warmup budget ablation. Fraction of total budget allocated to warmup PPO before expert averaging begins. Gymnasium, 1M steps, 5 seeds, mean \pm SE.

	0%	5%	10%	20%
<i>HalfCheetah</i>				
CAPO-Avg	1710 \pm 36	2443 \pm 417	2469 \pm 537	2706 \pm 473
CAPO	2203 \pm 496	2512 \pm 535	2190 \pm 482	2163 \pm 517
<i>Walker2d</i>				
CAPO-Avg	3695 \pm 521	3193 \pm 550	4089 \pm 226	3539 \pm 493
CAPO	3455 \pm 658	3394 \pm 484	3430 \pm 278	4263 \pm 405
<i>Ant</i>				
CAPO-Avg	1623 \pm 77	1417 \pm 180	1658 \pm 161	1696 \pm 369
CAPO	2231 \pm 65	2194 \pm 46	2267 \pm 196	2384 \pm 147

The optimal warmup fraction is task-dependent. For CAPO-Avg, 10% is best on Walker2d (4089) while 20% is best on HalfCheetah (2706) and Ant (1696). CAPO (LogOP) consistently outperforms CAPO-Avg across warmup fractions and environments, peaking at 5% on HalfCheetah (2512), 20% on Walker2d (4263) and Ant (2384). The default 10% used in the main results (Table 4) is a reasonable middle ground that avoids the worst-case on any environment for both methods.